18th International Symposium on Flow Visualization
Zurich, Switzerland, June 26-29, 2018

PRESSURE, TEMPERATURE AND VELOCITY DISTRIBUTIONS BEHIND AN NGV CASCADE BY FILTERED RAYLEIGH SCATTERING MEASUREMENTS

U. Doll[1,c], M. Dues[2], T. Bacci[3], A. Picchi[3], G. Stockhausen[4], C. Willert[4]

[1]Paul Scherrer Institute (PSI), Laboratory of Thermal Processes and Combustion, 5232 Villigen PSI, Switzerland
[2]ILA R&D GmbH, Karl-Heinz-Beckurts Str. 13, 52428 Juelich, Germany
[3]Dipartimento di Ingegneria industriale, University of Florence, 50139 Florence, Italy
[4]German Aerospace Center (DLR), Institute of Propulsion Technology, Measurement Technology, Linder Hoehe, 51147 Cologne, Germany
[c]Corresponding author: Tel.: +41 56 310 22 87; Email: ulrich.doll@psi.ch

KEYWORDS:
Main subjects: Aero-thermal flow characterization, intrusive impact
Fluid: turbomachinery flow, nozzle guide vane cascade
Visualization method(s): five-hole probe**,** filtered Rayleigh scattering
Other keywords: planar measurement, simultaneous, pressure, temperature, flow velocity

ABSTRACT: *The aero-thermal characterization of turbomachinery flows typically relies on well-proven conventional measurement technology such as pneumatic probes, hot-wire sensors or thermocouples. As these devices have to be introduced into the flow, they disturb the flow field at the actual measuring position. This is especially critical in the context of measurements in narrow flow channels typically found in turbomachinery applications. In this regard, both five-hole probe/temperature measurements as well as laser-optical filtered Rayleigh scattering measurements are carried out in order to characterize pressure, temperature and flow velocities downstream of a nozzle guide vane cascade with lean-burn combustion representative inflow distortions. By comparing the optical Doppler frequency-shifts measured with filtered Rayleigh scattering and calculated from five-hole probe velocity data, the study reveals a significant bias of the probe's velocity measurement caused by strong pressure gradients present in the airfoils' wake regions. In addition, passage flows are notably altered by the probe's intrusive impact on the flow. The study concludes that laser-optical filtered Rayleigh scattering diagnostics overcomes these shortcomings and is well suited to characterize aero-thermal flow properties in turbomachinery environments.*
.

1 Introduction

Lean burn combustion architectures are deemed a promising technological approach in order to meet ambitious emission targets and, at the same time, increase the overall efficiency of next generation aero-engines [1]. With the introduction of lean burn aero-engine combustors, enhanced flow distortions are to be expected at combustor-turbine interface. As a consequence of novel injector designs and the redirection of air mass within the combustion chamber, the flow approaching the turbine is highly swirled and turbulent and characterized by strong temperature gradients (hot streaks). The highly three-dimensional unsteady flow at the turbine inlet poses a significant challenge to commonly applied design procedures and underlines the need for high-quality experimental validation data [1, 2].

In this regard, a three-sector gas turbine rig made up of a combustor simulator and a nozzle guide vane (NGV) cascade was installed at the THT Lab (Laboratory of Technologies for High Temperature) of the University of Florence. Relevant temperature distortions, swirl as well as turbulence intensities are generated within the combustor simulator to mimic lean-burn representative flow conditions at the

turbine inlet plane [3]. Current experimental efforts aim on the characterization of the aero-thermal flow properties downstream of the NGV cascade.

Regarding planar laser-optical techniques, in particular PIV and, to a lesser extent, DGV were successfully applied to turbomachinery flows [4-9]. Despite their general ability to deliver time-resolved three-component velocity fields in turbomachinery environments, both PIV and DGV suffer from their susceptibility to laser scattering from surfaces, so that affected image areas have to be masked and thus cannot provide data in these areas [6, 7, 9]. In addition, seeding particles tend to deposit on windows, which, due to the degrading quality of optical access, in consequence leads to both reduced testing periods as well as a reduction in the signal-to-noise ratio. In this regard the filtered Rayleigh scattering technique (FRS) [10] may prove a valuable alternative to existing approaches. Extended by a frequency scanning method (FSM-FRS) [11, 12], the technique is capable of simultaneously acquiring time-averaged pressure, temperature and velocity maps. FRS relies on molecular scattering only; no seeding particles have to be added to the flow. In utilizing molecular absorption bands in the range of the excitation wavelength, laser stray light from surfaces can be effectively attenuated, yielding experimental results in the direct vicinity of highly luminous surfaces. The technique was already employed on several turbomachinery related applications, including multi-parameter measurements in air flows [11, 13] as well as in combustion environments [14, 15].

In this contribution, the FSM-FRS technique is used to investigate time-averaged pressure, temperature and velocity fields behind the NGV cascade of a three-sector gas turbine combustor simulator. FSM-FRS measurement results are compared against conventionally measured data acquired by means of a five-hole probe equipped with an additional temperature sensor.

2 Theoretical background of FSM-FRS

The FRS technique relies on molecular Rayleigh scattering, which holds information on density, pressure, temperature and flow velocity of gas molecules inside an observed probe volume with narrow-bandwidth laser light. As in many technical flows the region of interest typically lies inside some apparatus and must be observed through windows. In this environment stray laser light from channel boundaries or glass surfaces is superimposed onto the weak molecular scattering signal. In

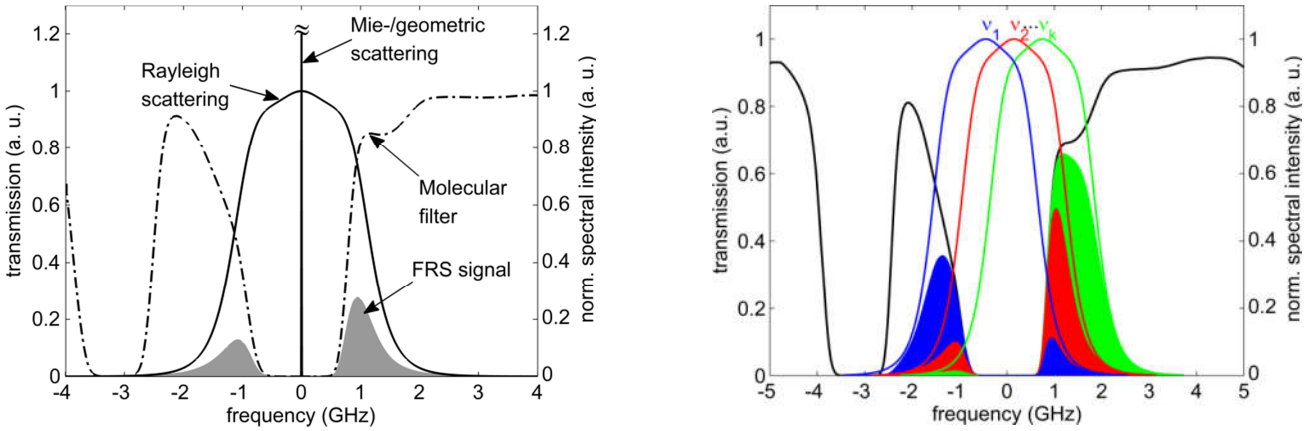

Fig. 1. Narrow linewidth laser light scattering is strongly attenuated by the molecular filter, while portions of Rayleigh scattering pass through (left). Frequency scanning method: The laser's output frequency is modulated multiple times along the molecular filter's transmission profile (right).

order to discriminate between laser light scattering from gas molecules on the one hand and stray light from surfaces or large particles entrained in the flow on the other, FRS utilizes molecular absorption to filter the latter from the measured signal. The concept of absorption filtering is illustrated in Fig. 1 (left): Particle (Mie) scattering as well as laser stray light originating from surfaces has similar spectral characteristics as the incident laser radiation, while Rayleigh scattering is spectrally broadened due to (mainly thermal) molecular motion. If now a molecular filter is placed in front of the detector, narrow-bandwidth surface and particle scattering is strongly attenuated while portions of Rayleigh scattering pass through and form the FRS signal (shaded areas in Fig. 1, left) [16].

FRS imaging typically utilizes cameras based on CCD/CMOS technology to record intensities scattered from the plane of interest. These devices cannot resolve the spectral characteristics holding the details on the measured quantities, but rather deliver one single integrated intensity value per sensor pixel (integral of the shaded areas in Fig. 1, left). The frequency scanning method offers a viable solution to restore the spectral information: as indicated in Fig. 1 (right), in FSM-FRS the laser's output frequency is tuned in discrete steps along the molecular filter's absorption profile. In acquiring images at each frequency step, intensity spectra at each sensor element are gathered. These intensity spectra can then be used to simultaneously retrieve time-averaged pressure, temperature and velocity maps [11, 12].

3 Experimental facility and optical arrangement

Fig. 2 (left) shows a sectional view of the non-reactive, three-sector combustor simulator rig coupled with a high pressure NGV cascade. The combustor simulator represents typical features of modern lean burn combustors in form of main-coolant mass flow split (65 %-35 %), effusion cooled liners without dilution holes and limited axial dimensions (~2.5 swirler diameters). The three-sector configuration was chosen in order to reduce the influence of the rig's lateral walls on the central sector flow field, which is the main target of the experimental survey. Pre-heated air at 423 K streams through three axial swirlers, which create a highly swirling flow in the adjacent chamber. Two separate lines at ambient temperature feed the effusion cooled inner and outer liner. In order to postpone the interaction between main flow and liner cooling, circular ducts of 55 mm length are installed on the swirlers. In this configuration, relevant temperature distortions combined with a high degree of swirl (±50°) as well as turbulence intensities (~30 %) are obtained at the combustor outlet/turbine inlet plane [3].

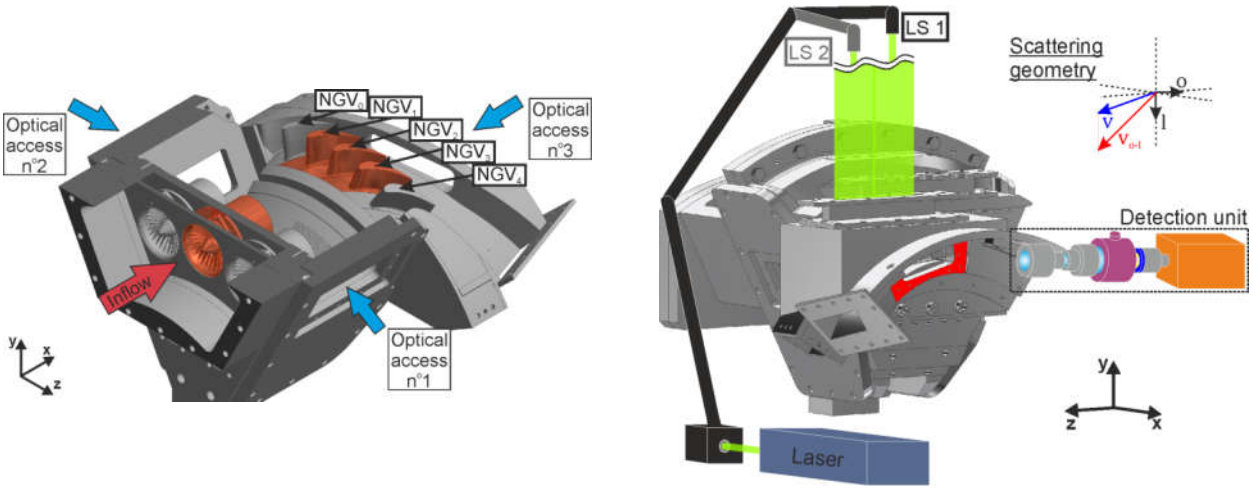

Fig. 2. Sectional view of the test rig's CAD model. The central sector is colored in orange, the red arrow points in flow direction, blue arrows indicate optical access to the rig (left). FSM-FRS setup: The laser beam is guided through an articulated mirror arm (black), formed into a light-sheet and enters the test rig from above along $\mathbf{l}$. To cover the whole visible cross section, the sheet is traversed in lateral direction. Scattered light is captured along $\mathbf{o}$ by a first lens (grey) and enters the detection unit, where it is transferred through the iodine cell (pink) as well as a bandpass filter (blue) by two lenses in retro-arrangement (grey) and finally is imaged onto the camera (orange) sensor. The detected Doppler frequency-shift is proportional the projection of the flow velocity $\mathbf{v}$ onto $\mathbf{o} - \mathbf{l}$ (v_{o-l}).

The NGV cascade consists of five vanes and six passages. The central vane has the leading edge aligned with the central swirler. Since only the central sector (i.e. two vane pitches) is subject of the investigation, only the three central airfoils ($NGV_{1\text{-}3}$ in Fig. 2,left) are film-cooled. Two dummy airfoils (NGV_0 and NGV_4) are installed on either side. The NGV cooling flow is provided by a further line at ambient temperature. A back-pressure valve is used to regulate the rig pressurization: a chamber pressure of 148 kPa and a pre-heat temperature of 150 °C result in an average Mach number at the cascade exit of 0.64. Optical access No. 3 is utilized to observe the plane of interest, which is located 0.25 axial chords (~9 mm) downstream of the NGV cascade's trailing edges.

Fig. 2 (right) shows a sketch of the FRS diagnostic's optical setup. The system relies on a Coherent Verdi V5 continuous wave laser, emitting single-frequency light at 532 nm with an adjustable output power of up to 5 W and a linewidth < 5 MHz. Two nested control loops based on a High Finesse WSU 10 wavelength-meter are installed to monitor and stabilize the laser's output frequency. By issuing control voltages onto two piezoelectric elements and thus altering the resonator's length, relative frequency deviations below 2 MHz are achieved. The output beam is directed via an articulated mirror arm (ILA GmbH) above the test rig, where it is formed into a light sheet of 45 mm width and < 0.5 mm thickness using an optical scanner arrangement designed for long camera exposures [17]. Laser power at the mirror arm exit is monitored by introducing a thin glass plate into the beam and directing the deflected beam portion onto a photodiode behind a rotating diffusion disc. The light sheet illuminates the plane of interest through a flange originally designed for five-hole probe traversing. To cover the whole visible area with laser light, the sheet optics is traversed in two positions in lateral direction.

The detection unit is composed of a first camera lens, capturing light scattered from the plane of interest. This is followed by two additional lenses in retro-arrangement, with a filter cell filled with molecular iodine and a bandpass filter (Barr, FWHM 1 nm) placed in-between. Finally, a third camera lens images the light transferred through the filter array onto the camera sensor (Hamamatsu C9100-13 EM-CCD). In order to maximize the visible area, the detection unit is oriented at 79° with respect to the measurement plane. Thus, two NGV pitches between vanes 2, 3 and 3, 4 are visible in the camera's field of view. Methods given in [18] are used to calibrate the camera position as well as to map the image data onto a Cartesian grid at a spatial resolution of 2 pixel/mm.

4 Results and discussion

In this section, time-averaged pressure, temperature and velocity results obtained by FSM-FRS measurements are compared to respective five-hole probe/temperature sensor data. In order to increase measurement accuracies, FSM-FRS data evaluation utilizes a correction method to account for laser induced background scattering as well as a calibrated Rayleigh lineshape model introduced in [19]. The thermal expansion of the rig during during heat-up along with associated changes of the optical path's efficiency are tackled by a modified measurement model, which, however, results in a lower pressure sensitivity of the FSM-FRS method [19]. The probe setup consists of a cobra-shaped five-hole probe (3 mm head size) with a J-type thermocouple installed at the probe stem. The device is traversed in the

plane of interest, resulting in a total of 335 grid points. Data is acquired over a period of 2 seconds at each position. Due to the probe's dimensions, obtaining results in the proximity of the channel's boundaries is not feasible. The probe is placed under a pre-swirl of 62.5° in order to reduce measured angles. A thorough calibration of the probe setup is carried out in a separate jet experiment, covering the relevant Mach number as well as swirl/yaw angle range.

Whereas temperatures and static pressures acquired with both methods can be directly compare to each other, the comparison of velocity data obtained by the five-hole probe with FSM-FRS measurement results relies on the optical Doppler frequency-shift. The scattering geometry of the optical setup

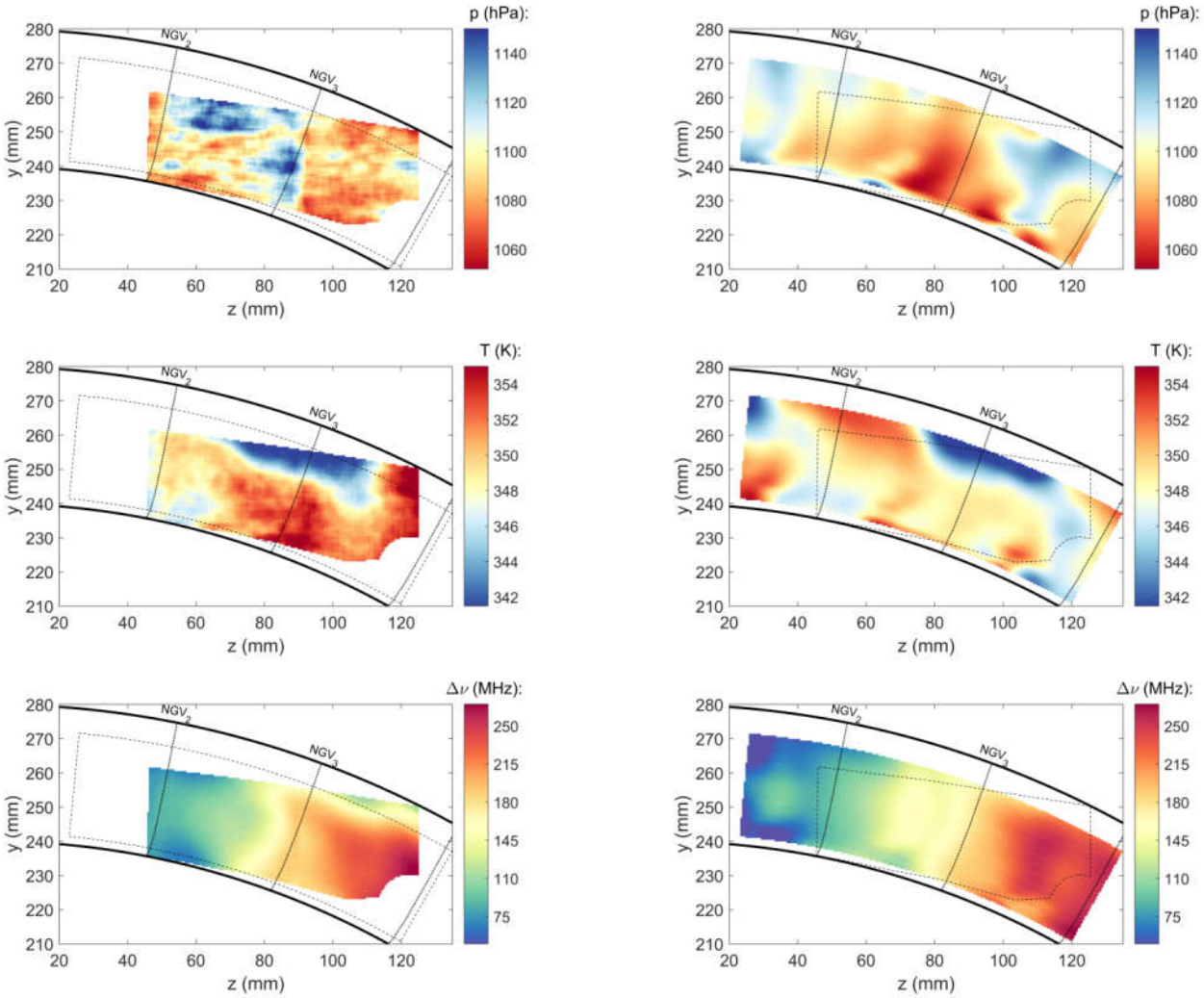

Fig. 3. Comparison of FSM-FRS (left) and five-hole probe (right) static pressure (top), temperature (middle) and Doppler frequency-shift (bottom) maps. Thick solid lines mark the upper (radius 280 mm) and lower (radius 240mm) channel boundaries, dashed lines indicate areas investigated by the alternate method and dotted lines denote NGV trailing edge positions projected onto the measurement plane. Five-hole probe maps are interpolated from the probe grid to FSM-FRS results resolution. Results of both methods are smoothed with a moving average filter (5 x 5 kernel size).

is depicted in the upper right corner of Fig. 2 (right). The Doppler frequency-shift measured by the FSM-FRS method is proportional to the velocity component along the bisector spanned by laser direction and observer position. Hence a single camera view resulting in a single Doppler frequency-shift is not sufficient to reconstruct a velocity vector field [13, 20]. To compare velocity results of both methods, the three-component velocity data obtained by the five-hole probe is converted into Doppler frequency-shifts by projecting the probe's velocity vector field onto the FSM-FRS scattering geometry.

Fig. 3 shows a comparison of static pressure, temperature as well as Doppler frequency-shift maps obtained with FSM-FRS and five-hole probe/temperature sensor, respectively. As indicated above, the probe's dimensions limit the minimal wall distance, whereas FSM-FRS results extend to the upper and lower boundaries. In observing the plane of interest through optical access No. 3 (see Fig. 2, left), part of the flow channel, which is accessible by the probe traverse, is obstructed from the camera view. Overall, results obtained with both methods exhibit good quantitative agreement for all shown quantities. Apparent differences in structure of the measured pressure, temperature and Doppler frequency-shift maps will be discussed below.

Both static pressure maps of FSM-FRS and five-hole probe measurements exhibit a similar absolute level of about 1100 hPa. Concerning the pressure field's structure, zones of heightened pressure between NGV vanes 2 and 3 are visible in the upper half of FSM-FRS results as well as, although less pronounced and shifted upwards, in five-hole probe data. However, a second zone of increased static pressure is visible in the center of FSM-FRS results is not apparent in five-hole probe pressure data, which exhibits a slight dropping at this location. The cause for the difference may lie in an insufficient correction of laser-induced background scattering. As the correction method introduced in [19] relies on interpolating a coarse grid of measured background intensities onto the complete imaged region, illuminated structured elements such as airfoil edges in the background are not well captured by the method. Hence the methodology leads to an erroneous correction of background intensities in affected image areas. In between vanes 3 and 4, the FSM-FRS static pressure distribution is almost constant, while the five-hole probe data is governed by a streak of heightened static pressure values. Temperature maps obtained by FSM-FRS and temperature sensor measurements are in good agreement in terms of structure as well as absolute value. Temperature dynamics is characterized by peak values in the range 350 to 355 K and a lower bound of about 340 K. A cold streak, beginning in the middle of NGV pitch 2-3 and extending into the region between vanes 3 and 4, is visible in both distributions. While the structure ends near the flow channel's radial centerline in FSM-FRS results, it extends until the lower bound of the probe traverse. Another cold spot near the lower end of NGV_2 is visible in both datasets. Regarding Doppler frequency-shifts measured by FSM-FRS and calculated from three-component five-hole probe velocity data, a good quantitative as well as qualitative agreement can be observed. The rise of absolute values from left to right is following the steady increase of v_y in lateral direction. Two regions, where differences between both maps are most pronounced, can be identified: first in the center near the trailing edge of NGV_3 where FSM-FRS results are governed by a steep gradient, while five-hole probe data in this region appears blurred. Second in the upper zone of NGV pitch 3-4 FSM-FRS data exhibits another steep gradient in radial direction, which in contrast is not evident in five-hole probe results.

The differences between five-hole probe/temperature sensor measurements are further characterized by radial centerline profiles of the measured quantities summarized in Fig. 4. Dashed-dotted lines mark the

NGVs' trailing edges, while the red transparent zones indicate the respective airfoils' wake regions [21, 22]. The static pressure curve measured by FSM-FRS exhibits strong spatial variations of 5% to 7% of the average level, which, however, are to be expected due to the reduced pressure sensitivity caused by the data evaluation procedure mentioned above. Besides a general agreement in magnitude between FSM-FRS and five-hole probe measurement results, no strong relation between both curves can be stated. Temperature profiles on the other hand confirm above findings of good agreement in structure as well as absolute level. However, the five-hole probe curve appears to be shifted from FSM-FRS results in z-direction by an amount of about 10 mm. This shift can be attributed to the differing positions of the FSM-FRS light sheet in the actual plane of interest and the temperature sensor's location, which is fixed to the probe stem and is therefore displaced x- as well as z-direction. With

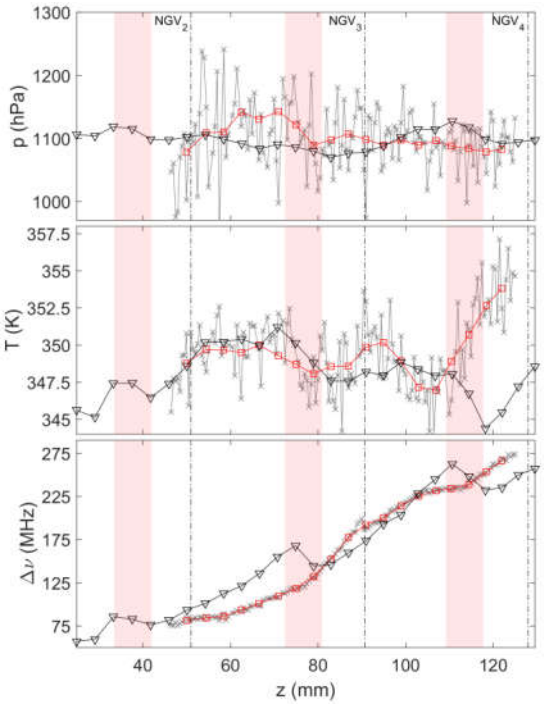

Fig. 4. Radial centerline profiles of static pressure, temperature as well as Doppler frequency-shift for FSM-FRS (gray, x) and five-hole probe/temperature sensor (black, ▽) measurement results. Red lines (□) represent FSM-FRS results mapped onto the five-hole probe measurement grid and resolution. Dashed-dotted lines mark NGV trailing edge positions projected onto the measurement plane, red transparent areas indicate respective wake regions.

regard to Doppler frequency-shifts, these exhibit the strongest dynamics of all measured quantities. FSM-FRS results start from 75 MHz on the left. The curve then steadily grows until it reaches a maximum of about 275 MHz on the right. Starting at a similar absolute level near the trailing edge of NGV_2, the five-hole probe's curve develops with differing slope towards the adjacent wake region, where it steeply drops towards the FSM-FRS profile. Outside of the wake, the five-hole probe data increases again and crosses the FSM-FRS profile, until it reaches the wake zone of NGV_3 where it drops below the FSM-FRS curve. The black curve then rises on a lower absolute level.

While the temperature measurements of both methods are in good agreement, aside from differences caused by the differing measuring locations, the FSM-FRS pressure data is not sufficient to assign observable differences to some intrusive impact of the five-hole probe, the sudden drop of Doppler

frequency-shift inside the airfoils' wake regions can clearly be attributed to erroneous probe measurements. It is well known from the literature that, when exposed to strong pressure gradients as they are present in airfoil wakes, these devices are prone to significant measurement error due to the spatial placement of the pressure taps on the probe geometry [23-25]. Regarding the differences between Doppler frequency-shift measured in the passages between two neighboring airfoil wakes, it is reasonable to assume a blocking impact of the five-hole probe's physical presence onto the flow field. However, as the flow downstream of the NGV cascade is highly three-dimensional, a single Doppler frequency-shift measured by non-intrusive FSM-FRS is not sufficient to pin down the actual effect of the probe on the flow structure.

5 Conclusion

The aero-thermal properties of the flow downstream of a combustor simulator coupled with a high pressure NGV cascade are characterized by means of conventional five-hole probe/temperature sensor measurements as well as laser-optical FSM-FRS diagnostics. Lean-burn representative flow distortions are simulated at the combustor outlet/turbine inlet plane, which are then propagated through the NGV airfoil passages.

The direct comparison of FSM-FRS and five-hole probe measurement data reveals good quantitative agreement in all measured quantities, while in terms of flow structure, certain differences are apparent. Due to an insufficient quality of FSM-FRS pressure results, which is caused by the data evaluation methodology applied, no further comment on the probe's intrusive impact on the static pressure field can be inferred on the basis of the available data. Temperatures measured with both methods, aside from a lateral shift, are in good agreement in terms of absolute value as well as topology. Doppler frequency-shifts (velocities), however, are significantly biased, on the one hand, by strong pressure gradients in the airfoil's wake regions, on the other hand, by the presence of the probe body itself.

Above findings reveal notable challenges when applying standard pneumatic probe-based technology in the characterization of highly three-dimensional flows in confined environments, as they are commonly found in applications related to turbomachinery. In this regard, laser optical FSM-FRS diagnostics presented herein proves a viable alternative in providing insight into the complex aero-thermal flow topology downstream of an NGV cascade with highly distorted inflow.

References

[1] R. von der Bank, S. Donnerhack, A. Rae, M. Cazalens, A. Lundbladh, and M. Dietz, "LEMCOTEC: Improving the Core-Engine Thermal Efficiency," in *ASME Turbo Expo 2014: Turbine Technical Conference and Exposition*, pp. V01AT01A001-V01AT01A001.

[2] M. Chevrier and H. Bertrand, "Full Aero-thermal Combustor-Turbine interactiOn Research (FACTOR) - Final Publishable Summary Report," 2017.

[3] T. Bacci, G. Caciolli, B. Facchini, L. Tarchi, C. Koupper, and J.-L. Champion, "Flowfield and Temperature Profiles Measurements on a Combustor Simulator Dedicated to Hot Streaks Generation," in *ASME Turbo Expo 2015: Turbine Technical Conference and Exposition*, pp. V05CT17A001-V05CT17A001.

[4] P. J. Bryanston-Cross, C. E. Towers, T. R. Judge, D. P. Towers, S. P. Harasgama, and S. T. Hopwood, "The Application of Particle Image Velocimetry (PIV) in a Short-Duration

Transonic Annular Turbine Cascade," *Journal of Turbomachinery,* vol. 114, no. 3, pp. 504-509, 1992.

[5] A. Fischer, L. Büttner, J. Czarske, M. Gottschall, K. Vogeler, and R. Mailach, "Investigation of the Tip Clearance Flow in a Compressor Cascade Using a Novel Laser Measurement Technique With High Temporal Resolution," *Journal of Turbomachinery,* vol. 134, no. 5, pp. 051004--051004-9-051004, 2012.

[6] A. Fischer, J. König, J. Czarske, C. Rakenius, G. Schmid, and H.-P. Schiffer, "Investigation of the tip leakage flow at turbine rotor blades with squealer cavity," *Experiments in Fluids,* vol. 54, no. 2, pp. 1462-1462, 2013.

[7] M. Voges, C. E. Willert, R. Mönig, M. W. Müller, and H.-P. Schiffer, "The challenge of stereo PIV measurements in the tip gap of a transonic compressor rotor with casing treatment," *Experiments in Fluids,* vol. 52, no. 3, pp. 581-590, 2012.

[8] M. P. Wernet, "Development of digital particle imaging velocimetry for use in turbomachinery," *Experiments in Fluids,* vol. 28, no. 2, pp. 97-115, 2000.

[9] J. Woisetschläger, N. Mayrhofer, B. Hampel, H. Lang, and W. Sanz, "Laser-optical investigation of turbine wake flow," *Experiments in Fluids,* vol. 34, no. 3, pp. 371-378, 2003.

[10] R. Miles and W. Lempert, "Two-dimensional measurement of density, velocity, and temperature in turbulent high-speed air flows by UV Rayleigh scattering," *Applied Physics B: Lasers and Optics,* vol. 51, pp. 1-7, 1990.

[11] U. Doll, G. Stockhausen, and C. Willert, "Endoscopic filtered Rayleigh scattering for the analysis of ducted gas flows," *Experiments in Fluids,* vol. 55, no. 3, pp. 1-13, 2014.

[12] J. Forkey, "Development and Demonstration of Filtered Rayleigh Scattering: a Laser Based Flow Diagnostic for Planar Measurement of Velocity, Temperature and Pressure," Princeton University, 1996.

[13] U. Doll, G. Stockhausen, and C. Willert, "Pressure, temperature, and three-component velocity fields by filtered Rayleigh scattering velocimetry," *Opt. Lett.,* vol. 42, no. 19, pp. 3773-3776, 2017.

[14] U. Doll, G. Stockhausen, J. Heinze, U. Meier, C. Hassa, and I. Bagchi, "Temperature Measurements at the Outlet of a Lean Burn Single-Sector Combustor by Laser Optical Methods," *Journal of Engineering for Gas Turbines and Power,* vol. 139, no. 2, pp. 021507-021507, 2017.

[15] M. Schroll *et al.*, "Flow Field Characterization at the Outlet of a Lean Burn Single-Sector Combustor by Laser-Optical Methods," *Journal of Engineering for Gas Turbines and Power,* vol. 139, no. 1, pp. 011503-011503, 2017.

[16] R. Miles, A. Yalin, Z. Tang, S. Zaidi, and J. Forkey, "Flow field imaging through sharp-edged atomic and molecular notch filters," *Measurement Science and Technology,* vol. 12, no. 4, pp. 442-442, 2001.

[17] I. Röhle and C. Willert, "Extension of Doppler global velocimetry to periodic flows," *Measurement Science and Technology,* vol. 12, no. 4, pp. 420-420, 2001.

[18] C. Willert, "Assessment of camera models for use in planar velocimetry calibration," *Experiments in Fluids,* vol. 41, no. 1, pp. 135-143, 2006.

[19] U. Doll, E. Burow, G. Stockhausen, and C. Willert, "Methods to improve pressure, temperature and velocity accuracies of filtered Rayleigh scattering measurements in gaseous flows," *Measurement Science and Technology,* vol. 27, no. 12, pp. 125204-125204, 2016.

[20] J. F. Meyers and H. Komine, "Doppler global velocimetry-A new way to look at velocity," in *Laser Anemometry-Advances and Applications 1991*, vol. 1, pp. 289-296.

[21] D. G. Ainley and G. C. R. Mathieson, *A Method of Performance Estimation for Axial-flow Turbines*. H.M. Stationery Office, 1951.
[22] B. Lakshminarayana and R. Davino, "Mean Velocity and Decay Characteristics of the Guidevane and Stator Blade Wake of an Axial Flow Compressor," *Journal of Engineering for Power,* vol. 102, no. 1, pp. 50-60, 1980.
[23] J. Aschenbruck, T. Hauptmann, and J. R. Seume, "Influence of a multi-hole pressure probe on the flow field in axial-turbines," in *11th European Conference on Turbomachinery Fluid Dynamics and Thermodynamics, ETC 2015*.
[24] H. T. Hoenen, R. Kunte, P. Waniczek, and P. Jeschke, "Measuring Failures and Correction Methods for Pneumatic Multi-Hole Probes," in *ASME Turbo Expo 2012: Turbine Technical Conference and Exposition*, pp. 721-729.
[25] C. Sanders, M. Terstegen, M. Hölle, P. Jeschke, H. Schönenborn, and T. Fröbel, "Numerical Studies on the Intrusive Influence of a Five-Hole Pressure Probe in a High-Speed Axial Compressor," in *ASME Turbo Expo 2017: Turbomachinery Technical Conference and Exposition*, pp. V02AT39A009-V02AT39A009.

Acknowledgements

The authors wish to gratefully acknowledge the financial support by FACTOR (Full Aerothermal Combustor-Turbine interactiOns Research). FACTOR is a Collaborative Project co-funded by the European Commission within the Seventh Framework Program (2010-2016) under Grant Agreement No. 265985.

Copyright Statement

The authors confirm that they, and/or their company or institution, hold copyright on all the original material included in their paper. They also confirm they have obtained permission, from the copyright holder of any third-party material included in their paper, to publish it as part of their paper. The authors grant full permission for the publication and distribution of their paper as part of the ISFV18 proceedings or as individual off-prints from the proceedings.